Ukrainian Journal of Remote Sensing
journal homepage: www.ujrs.org.ua

https://doi.org/10.36023/ujrs.2024.11.3.266

УДК 004.9:57

Classification of BPG-Based Lossy Compressed Noisy Images

G. A. Proskura*, V. V. Naumenko, V. V. Lukin

Department of Information and Communication Technologies, National Aerospace University, 61070 Kharkiv, Ukraine

Acquired remote sensing images can be noisy. This fact has to be taken into account in their lossy compression and classification. In particular, a specific noise filtering effect is usually observed due to lossy compression and this can be positive for classification. Classification can be also influenced by methodology of classifier learning. In this paper, we consider peculiarities of lossy compression of three-channel noisy images by better portable graphics (BPG) encoder and their further classification. It is demonstrated that improvement of data classification accuracy is not observed if a given image is compressed in the neighborhood of optimal operation point (OOP) and the classifier training is performed for the noisy image. Performance of neural network based classifier is studied. As demonstrated, its training for compressed remote sensing data is able to provide certain benefits compared to training for noisy (uncompressed) data. Examples for Sentinel data used in simulations are offered.

Keywords: image lossy compression; optimal operation point; BPG encoder, classification transform.

1. Introduction

Remote sensing (RS) from satellites, aircraft and drones has found numerous applications in recent years (Aiazzi et al., 2012; Chi et al., 2016; Vasilyeva et al., 2023). Acquired images' number and their mean size have the tendency to increase (Khorram et al., 2016). This leads to big data problems at all stages of image data processing including co-registration, storage, filtering, classification (Chi et al., 2016; Ma et al., 2015).

One way to solve the problems in RS data storage and transmission is to apply their compression (Hussain et al., 2018; Tao et al., 2018; Doss et al., 2020). As known, two main types of image compression techniques exist, namely, lossless and lossy (Hussain et al., 2018; Sayood et al., 2017). Lossless techniques are known to introduce no distortions into data. However, the compression ratio (CR) provided by them is often inappropriate. Thus, lossy compression has become the main tool to provide a desired and variable CR or quality of compressed RS data (Sayood et al., 2017; Li et al., 2020; Proskura et al., 2020). Increased CR might result in worse quality of compressed RS data. Because of this, a reasonable trade-off between the attained CR and compressed data quality has to be found for each particular image (Tao et al., 2018; Christophe et al., 2011; Makarichev et al., 2022). This trade-off depends on an application analyzed, a coder (compression method) applied, properties of an image to be compressed, priority of requirements to compression and their further processing (Makarichev et al., 2022), etc. Here we consider the influence of lossy compression on image classification accuracy.

If an image to be compressed is (practically) noise-free, the general tendencies are the following. CR increase generally leads to worse classification where overall probability of correct classification P_{cc} slightly reduces with CR increase if distortions are invisible and starts to diminish quickly if distortions become visible (Proskura et al., 2020; Makarichev et al., 2022). Note that coder parameters for just noticeable distortions (JND) can be predicted (Bondžulić et al., 2021). CR for JND depends on image complexity where CR for complex structure images can be by several times smaller than for simple structure images for the same quality of compressed RS data. Note that CR also depends on a coder used. In this sense, the better portable graphics (BPG) encoder (Yee et al., 2017; Albalawi et al., 2016) is able to provide significantly better performance characteristics compared to JPEG2000 (Taubman et al., 2013) and some other modern lossy compression techniques. This is one of the main reasons why we consider just this encoder in our studies.

In practice, there are cases when an image to be compressed is noisy (Chatterjee and Milanfar, 2010). Then, image lossless and lossy compression has several specific features. First, CR for lossless compression is only slightly larger than unity since bytes are spent on noise preservation. In turn, specific noise filtering effect is observed for lossy compression of noisy images. This effect was first discovered almost 30 years ago (Al-Shaykh et al., 1998; Chang et al., 1997) for JPEG. Later it was studied for other lossy compression techniques (Zemliachenko et al., 2015) and, in particular, for the BPG encoder (Kovalenko et al., 2021; Lukin et al., 2022). The BPG-based encoder is preferable for lossy compression of noisy images compared to many modern

*E-mail: g.proskura@khai.edu

encoders (Kryvenko et al., 2024) and this is the second reason for paying the attention to its consideration. The third advantage of this encoder is that position of optimal operation point (OOP) for it can be easily determined for a priori known or pre-estimated noise characteristics (Lukin et al., 2022) where there exist blind methods for noise characteristic evaluation (Selva et al., 2021; Abramova et al, 2024).

OOP (Al-Shaykh et al., 1998; Zemliachenko et al., 2015), in general, is a parameter that controls compression (PCC) for which the compressed image is closer to the corresponding noise-free image than original (noisy) image according to a considered metric characterizing similarity. As PCC, different coders use quality factor, bits per pixel, quantization step and so on. The BPG encoder employs the parameter Q that is non-negative and integer. There is a strict dependence between Q in OOP and variance of additive noise (Lukin et al., 2022). Thus, under condition of a priori known noise variance or its pre-estimation with appropriate accuracy, compression in OOP neighborhood can be realized in fully automatic mode.

Lossy compression in OOP has several advantages. First, a rather large CR can be provided. Second, it has been shown for coders based on discrete cosine transform that compression in OOP is able to produce a larger F_{cc} than F_{cc} for classification of original (noisy) image (Lukin et al., 2008). However, peculiarities of classification have not been yet studied for noisy multichannel RS images compressed by the BPG encoder.

As a starting point, we consider the case of three-channel RS image corrupted by additive white Gaussian noise (AWGN) with variance equal in all three component images. Such an approach allows using results and recommendations obtained in our previous papers (Lukin et al., 2022) intended on reaching compression in OOP. The paper novelty consists in the following. First, we analyze component-wise compression of multichannel noisy RS images with emphasis on accuracy of their classification. Second, we demonstrate that lossy compression in OOP neighborhood can be expedient from the viewpoint of providing high F_{cc} if OOP exists, i.e. for images of a quite simple structure corrupted by rather intensive noise. We also analyze the cases of complex structure image and, in addition to F_{cc}, study probabilities of correct classification for separate classes. Third, we compare two opportunities of classifier learning – for noisy image and for compressed RS data – and show that the latter option can be beneficial.

2. Used criteria and image/noise model

As told above, we deal with lossy compression of noisy three-channel images. Noise in RS data can be due to different reasons (Abramova et al., 2023; Chatterjee et al., 2010) including a limited time of signal registration, principle of imaging system operation, etc. Respectively, it can be additive or signal dependent. Below, we concentrate on considering the AWGN model (Chatterjee et al., 2010) used as a starting point in our research. According to it, one has

$$I_{kij}^{noisy} = I_{kij}^{true} + n_{kij}, \quad (1)$$

where I_{kij}^{noisy} denotes the noisy ij-th pixel value, I_{kij}^{true} is the true ij-th pixel value, n_{kij} is the value of AWGN having zero mean and variance σ^2, $k = 1,\ldots3$ denotes the channel index. If noise is signal-dependent, proper variance stabilizing transforms applied before RS data compression can result in getting data for which the model (1) is valid. We assume that noise variance is the same in all three components and it is *a priori* known or accurately pre-estimated (Selva et al., 2021).

Quality of original noisy image can be described in different ways where the most typical is peak signal-to-noise ratio ($PSNR^n$) determined as

$$MSE_k^n = \sum_{i=1}^{I}\sum_{j=1}^{J}(I_{kij}^n - I_{kij}^{true})^2/(IJ), \quad (2)$$

$$PSNR_k^n = 10\log_{10}\left(\frac{255^2}{MSE_k^n}\right) = 10\log_{10}\left(\frac{255^2}{\sigma^2}\right), \quad (3)$$

where I and J describe the image dimensions. Here and below we assume that our image is represented as 8-bit data in each component. To be visible, the AWGN (supposed uncorrelated in component images) should have $\sigma^2 \approx 20$ if an image has a simple structure and $\sigma^2 \approx 25$–30 for complex structure images (Ponomarenko et al., 2015). This corresponds to $PSNR_k^n \approx 35$ dB and $PSNR_k^n \approx 34$ dB, respectively. Thus, in our simulations, we consider the noise variance equal to 25 and larger.

To simulate natural scenes, we have taken two almost noise-free RS images composed of three components of visible range of Sentinel-2 multispectral data (see Fig. 1). These images were acquired at the end of August in 2019. The image fragments have the size of 512×512 pixels. The reasons for using these data were the following. First, the images are of different complexity where the image in Fig. 1, a is for country side (Kharkiv region) and it contains rather large quasi-homogeneous regions whilst the image in Fig. 1, b has complex structure and it corresponds to the North part of Kharkiv. Second, we knew cover types (classes) – these data were available from topographic maps and we knew these regions well (the second region is close to our University). Third, in both cases, four classes – Urban, Water, vegetation, and Bare Soil could be quite easily identified.

a b

Fig. 1. Image fragments used in simulations: SS1 – Staryi Saltiv (a), SS2 – North Kharkiv (b)

It is worth explaining what is OOP. Let us consider dependences $PSNR_k^{ct}(Q)$ where $PSNR_k^{ct}$ is calculated between the a k-th true and compressed component

images for a set of Q values that for the BPG encoder vary from 1 (almost no distortions with small CR) to 51 (considerable CR and introduced distortions) with $Q \approx 27$ that corresponds to distortion visibility threshold. Recall here that in the case of compressing a single channel noisy image or component-wise compression of multichannel image the parameter Q for OOP is determined as

$$Q_{OOP} = 14.9 + 20\log_{10}(\sigma). \quad (4)$$

Then, for σ^2 equal to 25, 50, and 100 considered in our simulations, one has Q_{OOP} approximately equal to 29, 32, and 35, respectively.

One set of the obtained dependences is demonstrated in Fig. 2 for the test images in Fig. 1 contaminated with AWGN with $\sigma^2 = 100$ as well as two other images (SS3 and SS4 where the image SS3 is similar to SS1 and SS4 is similar to SS2). The plots for all three components are given. The data analysis shows the following. First, the plots for components are the same image are similar to each other. This is not surprising since component images of multispectral data are usually highly correlated (similar). Second, there are quite many curves that all have maxima observed for $Q_{OOP} = 35$ and this is in agreement with (4). Third, maximal values $PSNR_k^{ct}$ observed in OOP can be significantly larger than $PSNR_k^n = 28$ dB. Then, compression in OOP seems reasonable. Meanwhile, there are also one curve having local maximum and two curves having no maxima at all (they are monotonically decreasing) – all observed for the image SS4 which has the most complex structure.

The analysis carried out for two other values of the noise variance additionally shows that OOP is observed not for all images and noise variance values. Usually, it is possible to expect OOP existence for images having quite simple structure and/or contaminated by a rather intensive noise. OOP existence can be predicted before compressing a given image using the approach based on analysis of DCT coefficient statistics in 8x8 blocks (Lukin et al., 2022). If OOP is (supposed) absent, it is reasonable to use lossy compression with Q smaller than Q_{OOP} (4). For example, it can be recommended to use $Q_{rec} = Q_{OOP} - 4$ or $Q_{rec} = 27$ or 28 to have invisibility of introduced distortions.

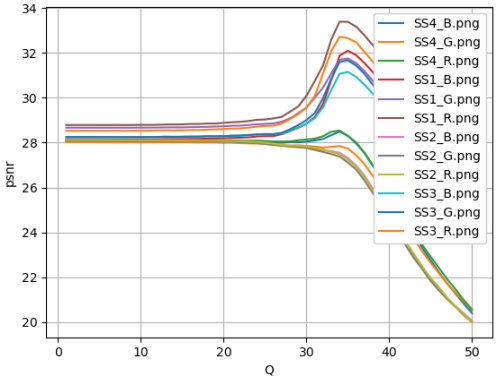

Fig. 2. Dependencies $PSNR_k^{ct}(Q)$ for the coder BPG applied to the test images SS1-SS4 corrupted by AWGN with variance equal to 100 component-wise ($PSNR^n \approx PSNR_k^{ct}$ $(Q = 1)$ is of about 28 dB)

3. Considered coder and classifier

3.1. BPG encoder

As said above, in this paper, we focus on Better Portable Graphics encoder. The BPG encoder relies on the High Efficiency Video Coding (HEVC) method proposed by Fabrice Bellard as the open-source code (https://bellard.org/bpg/). This image compression method aims to replace the JPEG format due to several useful properties. First, it has significantly better performance producing higher quality for the same size of compressed data. It has lossless and lossy compression and is supported by most Web browsers. In addition, the BPG encoder supports the same chroma formats as JPEG, namely, grayscale, YCbCr 4:2:0, 4:2:2, 4:4:4, and several color spaces.

In application to compressing multichannel images, several options are possible. The simplest among them is to apply compression component-wise. Other ones deal with using aforementioned chroma formats. In this paper, we relied on the former approach as the starting point of using the BPG encoder for lossy compression of multichannel noisy RS images. Other approaches can be studied in the future.

3.2. Neural network classifier

For three-channel RS images, different approaches to their classification can be applied (Proskura et al., 2020; Makarichev et al., 2022). Based on the earlier obtained results (Proskura et al., 2020), we have used a neural network (NN) classifier applied pixel-wise. Its performance depends on several factors including the NN type and structure, methodology of training, etc.

The data to be processed have a direct impact on the choice of a neural network structure. As mentioned above, four main classes have been identified for both images considered: Urban, Water, Vegetation, and Bare Soil. Image fragments shown in Figures 3 and 4 were selected for training and verification of the classifier.

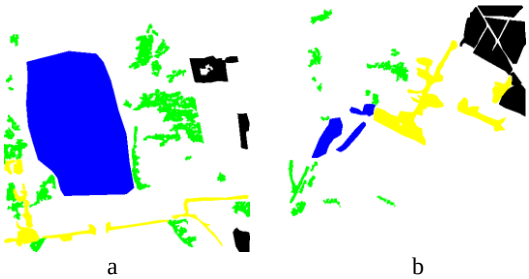

a b

Fig. 3. Fragments employed for the classifier training for the images SS1 (a) and SS2 (b)

a b

Fig. 4. Fragments employed for the classifier verification for the images SS1 (a) and SS2 (b)

The training and the verification samples sizes are given in Tables 1 and 2.

Table 1. The training and verification sample sizes for the test image SS1

Class	Training samples sizes, pixels	Verification samples sizes, pixels
Urban	7441	12154
Water	52310	96852
Vegetation	19936	38258
Bare Soil	1841304	1842906

Table 2. The training and verification sample sizes for the test image SS2

Class	Training samples sizes, pixels	Verification samples sizes, pixels
Urban	11469	28040
Water	4201	7117
Vegetation	5993	6032
Bare Soil	1850089	1854133

As discussed in (Lukin et al., 2023), for small sample sizes it is advisable to use a feedforward neural network, i.e. multilayer perceptron (MLP). The developed neural network includes 4 hidden layers containing 64, 32, 16, and 8 neurons, respectively, and an output layer. Hidden layers use the activation function ReLU, which is a nonlinear function that transforms the input value into a value between 0 and positive infinity.

$$\mathrm{ReLU}(x) = \max(0,x).$$

ReLU is characterized by high performance because it is a simple and has fast operation, which allows speeding up the learning process when using it in hidden layers. The output layer uses the Softmax activation function. The Softmax function curve has the property that the probability of any element in the vector increases if the values of other elements decrease, which allows this function to be used for multi-class classification.

To train MLP, the RMSProp optimizer was used, which is a modernized error backpropagation algorithm. The sparse categorical cross-entropy loss function has been utilized as a loss function, since it has demonstrated good results in multi-class classification.

Figure 5 shows the loss function and accuracy of our MLP depending on epoch number. It can be seen that the best result is observed around the 35th epoch.

Consider the metrics used to assess the quality of a classification. To evaluate the quality of the algorithm we have used an aggregated *F*-measure quality criterion representing the average harmonic precision and recall:

$$F = 2 \cdot \frac{precision \cdot recall}{precision + recall}.$$

Precision can be introduced as the proportion of objects that are classified by the classifier as positive and are actually positive. Recall shows how many objects of a full class of all positive objects the algorithm found. So, recall demonstrates the algorithm's ability to detect a given class in general, and precision shows its ability to distinguish this class from other classes.

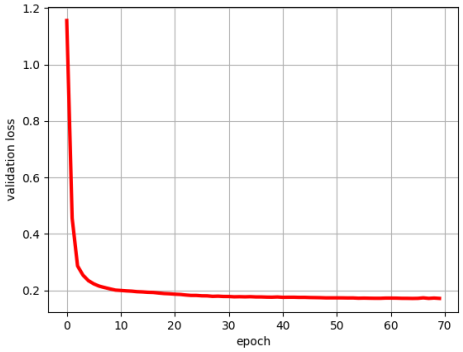

a)

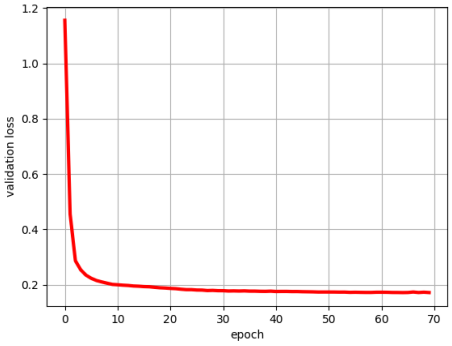

b)

Fig. 5. MLP loss function (a) and accuracy (b) depending on the number of epochs

For each image, *F*-measures were obtained when trained on the original image F_{cc}^{n} and when trained on the compressed image F_{cc}^{c}, as well as the corresponding *F*-measures for classes $F_{m}^{n}, m = 1,...,4$ and $F_{m}^{c}, m = 1,...,4$, where *m* is the class index and 1 corresponds to Urban, 2 – Water, 3 – Vegetation and 4 – Bare Soil.

4. Analysis of the obtained results

4.1. Data for the simple structure image

The obtained results are collected in Table 2. The values of *Q* that correspond to OOP for the corresponding noise variance are marked by Bold. Analysis shows the following:

1) The total F_{cc} is quite large (exceeds 0.9 for $\sigma^2 = 25$), Case 1, but this is mainly due to high F_2^c for Class 2 (Water); for other classes the probabilities are significantly smaller;

2) If noise is more intensive ($\sigma^2 = 50$, Case 5, and $\sigma^2 = 100$, Case 9), the total F_{cc} decreases; probabilities for particular classes diminish too;

3) Lossy compression leads to reduction of the total F_{cc}, this reduction is especially large for the largest considered $Q = 35$; probabilities for particular classes steadily decrease as well; in OOP according to PSNR, there is no OOP according to the total F_{cc};

4) The classifier learning for compressed data allows improving the classification results – compare the data for Case 13 to data for Case 2, the results for Case 14 to the results for Case 7, the data for Case 15 to the data for Case 12. The largest improvement is observed for the Cases 12 and 15 – F_{cc}^{c} has improved by 0.31.

Table 2. Classification data for the test image SS1

Case	Noise variance	Image used for training	Image used for classification	F_1	F_2	F_3	F_4	Total F_{cc}
1	25	Noisy	Noisy	0.75	0.97	0.86	0.73	**0.92**
2	25	Noisy	Compressed with Q = 29	0.75	0.82	0.64	0.63	**0.75**
3	25	Noisy	Compressed with Q = 32	0.71	0.77	0.58	0.55	**0.69**
4	25	Noisy	Compressed with Q = 35	0.68	0.69	0.52	0.47	**0.62**
5	50	Noisy	Noisy	0.68	0.95	0.77	0.65	**0.87**
6	50	Noisy	Compressed with Q = 29	0.60	0.76	0.58	0.36	**0.65**
7	50	Noisy	Compressed with Q = 32	0.48	0.67	0.53	0.26	**0.57**
8	50	Noisy	Compressed with Q = 35	0.44	0.59	0.48	0.21	**0.49**
9	100	Noisy	Noisy	0.55	0.91	0.66	0.57	**0.82**
10	100	Noisy	Compressed with Q = 29	0.43	0.75	0.53	0.24	**0.62**
11	100	Noisy	Compressed with Q = 32	0.34	0.62	0.46	0.19	**0.49**
12	100	Noisy	Compressed with Q = 35	0.27	0.51	0.42	0.16	**0.40**
13	25	Compressed with Q = 29	Compressed with Q = 29	0.75	0.93	0.73	0.68	**0.86**
14	50	Compressed with Q = 32	Compressed with Q = 32	0.62	0.88	0.58	0.47	**0.78**
15	100	Compressed with Q = 35	Compressed with Q = 35	0.41	0.83	0.42	0.22	**0.71**

4.2. Data for the complex structure image

The obtained results are collected in Table 2. Analysis allows drawing the following conclusions:

1) The total F_{cc} for σ^2 = 25 is smaller than for simple structure image (compare the data for Cases 1 in Tables 2 and 3; all classes are recognized not well enough;

2) If noise intensity increases (σ^2 = 50, Case 5, and σ^2 = 100, Case 9), the total F_{cc} diminishes; probabilities for particular classes become smaller too;

3) Lossy compression results in reduction of F_{cc}, especially for Q = 35; probabilities for particular classes steadily decrease as well; OOPs according to the total F_{cc} are not observed;

4) The classifier training for the compressed data improves the classification – compare the data for Cases 13 and 2, Case 14 and Case 7, Cases 15 and 12, respectively.

Table 3. Classification data for the test image SS2

Case	Noise variance	Image used for training	Image used for classification	F_1	F_2	F_3	F_4	Total F_{cc}
1	25	Noisy	Noisy	0.84	0.64	0.60	0.86	**0.79**
2	25	Noisy	Compressed with Q = 29	0.79	0.47	0.52	0.75	**0.70**
3	25	Noisy	Compressed with Q = 32	0.78	0.38	0.48	0.68	**0.67**
4	25	Noisy	Compressed with Q = 35	0.77	0.37	0.43	0.57	**0.63**
5	50	Noisy	Noisy	0.76	0.42	0.54	0.74	**0.70**
6	50	Noisy	Compressed with Q = 29	0.72	0.25	0.45	0.68	**0.63**
7	50	Noisy	Compressed with Q = 32	0.68	0.24	0.40	0.55	**0.56**
8	50	Noisy	Compressed with Q = 35	0.66	0.17	0.35	0.48	**0.53**
9	100	Noisy	Noisy	0.68	0.32	0.47	0.66	**0.62**
10	100	Noisy	Compressed with Q = 29	0.65	0.22	0.40	0.60	**0.56**
11	100	Noisy	Compressed with Q = 32	0.62	0.20	0.32	0.46	**0.49**
12	100	Noisy	Compressed with Q = 35	0.60	0.16	0.29	0.43	**0.47**
13	25	Compressed with Q = 29	Compressed with Q = 29	0.81	0.57	0.54	0.78	**0.74**
14	50	Compressed with Q = 32	Compressed with Q = 32	0.71	0.18	0.41	0.65	**0.61**
15	100	Compressed with Q = 35	Compressed with Q = 35	0.56	0.05	0.29	0.57	**0.51**

4.3. General tendencies and examples

Let us list and illustrate the general tendencies. First, if noise variance increases and classification is applied to uncompressed image (Cases 1, 5, and 9; classification maps in Figures 6, a, d, and e), classification maps become more "noisy" too. However, prolonged details are preserved (see the right part of the maps). Second, lossy compression leads to obtaining better classification results in homogeneous regions (vegetation, water surface) but fine details are partly lost – compare the maps in Fig. 6, a and 6, c to the map in Fig. 1, b. In addition, quite many misclassifications appear – many pixels are classified as Water instead of Vegetation in the urban region. This can be due to the fact that the classes Water and Vegetation are close for the image in Fig. 1, b since the water was "in blossom" in August when the image was acquired. Third, if noise is intensive and Q is large, classification maps occur to be of very low quality (Fig. 6, f).

Thus, one should keep in mind that noise and distortions due to lossy compression of noisy images

usually lead to significant misclassifications, especially if noise is intensive and/or Q is large (that corresponds to relatively large compression ratio).

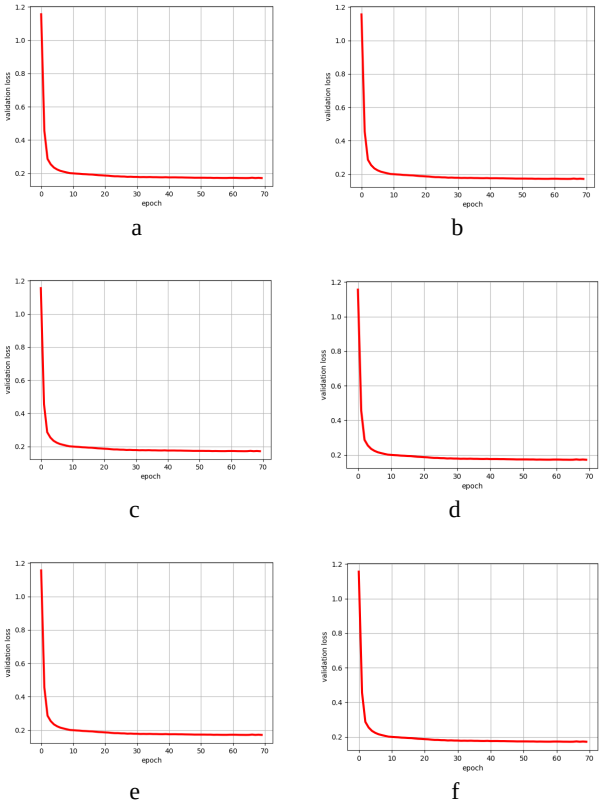

Fig. 6. Classification results for several Cases (see details in Table 3): a) Case 1; b) Case 2; c) Case 4; d) Case 5; e) Case 9; f) Case 12

One might think that aforementioned effects take place only for complex structure images. Fig. 7 shows examples of classification maps for the image in Fig. 1, a. In Fig. 7, a, the map is obtained for the image with $\sigma^2 = 25$ for which training and classification have been performed (Case 1 in Table 2). The result is good enough although there are misclassifications between Water and Vegetation classes. In turn, Fig. 7, b shows the map obtained for compressed image ($Q = 35$) where training was done for uncompressed image with $\sigma^2 = 100$ (Case 12 in Table 1). As one can see, small details (dam and roads) are partly lost and the classification results are of low quality.

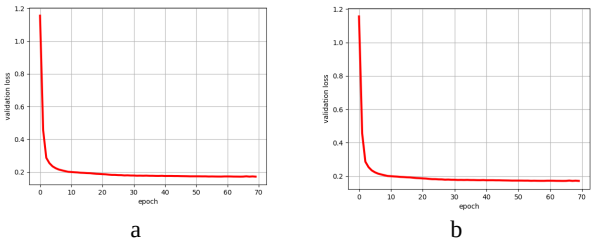

Fig. 7. Classification results for several Cases (see details in Table 1): a) Case 1; b) Case 12

5. Conclusions and future work

The task of pixel-wise classification of noisy three-channel images subject to lossy compression is considered. It is shown that both noise and distortions due to lossy compression result in degradation of classification where this degradation can be significant for intensive noise and high compression ratio. The situation can be partly improved if the classifier training is carried out for compressed data and/or if compression is performed without visual losses. In the future, we also plan to consider the opportunities of noisy image pre- or post-filtering to improve classification.

This work is supported by the National Research Foundation in Ukraine within the project № 2023.04/0039 “Geospatial monitoring system for the war impact on the agriculture of Ukraine based on satellite data” (2024–2025).

References

Abramova, V., Abramov, S., Abramov, K., Vozel, B. (2024). *Blind Evaluation of Noise Characteristics in Multichannel Images. Studies in Systems, Decision and Control* (pp. 209–229) Cham: Springer. doi: 10.1007/978-3-031-43579-9_4.

Aiazzi, B., Alparone, L., Baronti, S., Lastri, C., Selva, M. (2012). Spectral distortion in lossy compression of hyperspectral data. *Journal of Electrical Computer Engineering*. Article ID 850637, 8. https://doi.org/10.1155/2012/850637.

Albalawi, U., Mohanty, S. P., Kougianos, E. (2016). *Energy-Efficient Design of the Secure Better Portable Graphics Compression Architecture for Trusted Image Communication in the IoT*. 2016 IEEE Computer Society Annual Symposium on VLSI (ISVLSI), 302–307. doi: 10.1109/ISVLSI.2016.21.

Al-Shaykh, O. K., Mersereau, R. M. (1998). Lossy compression of noisy images. *IEEE Transactions on Image Processing*, 7(12), 1641–1652. doi: 10.1109/ 83.730376.

Bondžulić, B., Stojanović, N., Petrović, V., Pavlović, B., Miličević, Z. (2021). Efficient Prediction of the First Just Noticeable Difference Point for JPEG Compressed Images. *Acta Polytechnica Hungarica*, 18(8), 201–220. doi:10.12700/APH.18.8.2021.8.11.

Chang, S. G., Yu, B., Vetterli, M. (1997). Image denoising via lossy compression and wavelet thresholding. *Proceedings of International Conference on Image Processing*, 1, 604–607. doi: 10.1109/ICIP.1997.647985.

Chatterjee, P., Milanfar, P. (2010). Is Denoising Dead? *IEEE Transactions on Image Processing*, 19(4), 895–911. doi: 10.1109/TIP.2009.2037087.

Chi, M., Plaza, A., Benediktsson, J. A., Sun, Z., Shen, J., Zhu, Y. (2016). Big data for remote sensing: Challenges and opportunities. *Proceedings of the IEEE*, 104(11), 2207–2219. doi: 10.1109/JPROC.2016.2598228.

Christophe, E., Prasad, S., Bruce, L., Chanussot, J. (eds) (2011). Hyperspectral Data Compression Tradeoff. *Optical Remote Sensing. Augmented Vision and Reality*. doi:10.1007/978-3-642-14212-3_2.

Doss, S., Pal, S., Akila, D., Jeyalaksshmi, S., Jabeen, T. N., Suseendran, G. (2020). Satellite image remote sensing for identifying aircraft using SPIHT and NSCT. *IEEE Signal processing magazine*, 7(5), 631–634.

Hussain, A. J., Al-Fayadh, A., Radi, N. (2018). Image compression techniques: A survey in lossless and lossy algorithms. *Neurocomputing*, 300, 44–69. doi:10.1016/j.neucom.2018.02.094.

Kovalenko, B., Lukin, V., Naumenko, V., Krivenko S. (2021). *Analysis of noisy image lossy compression by BPG using visual quality metrics*. 2021 IEEE 3rd International

Conference on Advanced Trends in Information Theory (ATIT), 20–25. doi:10.1109/ATIT54053.2021.9678575.

Khorram, S., Van der WieleFrank, C. F., Koch, F. H., Nelson, S. A. C., Potts, M. D. (2016). Future Trends in Remote Sensing. *Principles of Applied Remote Sensing*, 277–285.

Kryvenko, S., Lukin, V., Vozel, B. (2024). Lossy Compression of Single-channel Noisy Images by Modern Coders. *Remote Sensing*, 16, 2093, 1–19. doi:10.3390/rs16122093.

Li, F., Krivenko, S., Lukin, V. (2020). *Adaptive two-step procedure of providing desired visual quality of compressed image*. Proceedings of the 2020 4th International Conference on Electronic Information Technology and Computer Engineering, 407–414. doi: 10.1145/3443467.3443791.

Lukin, V., Ponomarenko, N., Zelensky, A., Kurekin, A., Lever, K. (2008). Compression and classification of noisy multichannel remote sensing images. *Proc. SPIE 7109, Image and Signal Processing for Remote Sensing*, XIV, 1–12. doi:10.1117/12.799497.

Lukin, V., Kovalenko, B., Kryvenko, S., Naumenko, V., Vozel, B. (2022). Prediction of Optimal Operation Point Existence and Its Parameters in BPG-Based Automatic Lossy Compression of Noisy Images. *Current Overview on Science and Technology Research*, 9, 1–36. doi:10.9734/bpi/costr/v9/4316A.

Ma, Y., Wu, H., Wang, L., Huang, B., Ranjan, R., Zomaya, A., Jie, W. (2015). Remote sensing big data computing: Challenges and opportunities. *Future Generation Computer Systems*, 51, 47–60. doi:10.1016/j.future.2014.10.029.

Makarichev, V., Vasilyeva, I., Lukin, V., Vozel, B., Shelestov, A., Kussul, N. (2021). Discrete Atomic Transform-Based Lossy Compression of Three-Channel Remote Sensing Images with Quality Control. *Remote Sens*, 14(1), 125. doi:10.3390/rs14010125.

Ponomarenko, N., Lukin, V., Astola, J., Egiazarian, K. (2015). *Analysis of HVS-metrics' properties using color image database TID2013*. International Conference on Advanced Concepts for Intelligent Vision Systems, 613–624. doi:10.1007/978-3-319-25903-1_53.

Proskura, G., Vasilyeva, I., Li, F., Lukin, V. (2020). *Classification of Compressed Multichannel Images and Its Improvement*. Proceedings of the 30th International Conference Radioelektronika, 62–67. doi:10.1109/radioelektronika49387.2020.9092371.

Sayood, K. (2017) *Introduction to data compression*. San Francisco: Morgan Kaufmann. ISBN: 978-0-12-415796-5.

Selva, E., Kountouris, A., Louet, Y. (2021). *K-Means Based Blind Noise Variance Estimation*. 2021 IEEE 93rd Vehicular Technology Conference (VTC2021-Spring), 1–7. doi:10.1109/VTC2021-Spring51267.2021.9449072.

Tao, D., Di, S., Liang, X., Chen, Z., Cappello, F. (2018). *Fixed-PSNR Lossy Compression for Scientific Data*. 2018 IEEE International Conference on Cluster Computing (CLUSTER), 314–318. doi:10.48550/arXiv.1805.07384.

Taubman, D. S., Marcellin, M. W. (2013). JPEG2000: image compression fundamentals, standards, and practice.

Vasilyeva, I., Lukin, V., Kharchenko, V., Nereta, A. (2023). *Combined Processing of Satellite and UAV Data to Increase the Classification Reliability*. Proceedings of the 4th International Workshop on Intelligent Information Technologies & Systems of Information Security, 539–552. https://ceur-ws.org/Vol-3373/paper37.pdf.

Yee, D., Soltaninejad, S., Hazarika, D., Mbuyi, G., Barnwal, R., Basu, A. (2017). *Medical image compression based on region of interest using better portable graphics (BPG)*. 2017 IEEE International Conference on Systems, Man, and Cybernetics (SMC), 216–221. doi:10.1109/SMC.2017.8122605.

Zemliachenko, A., Abramov, S., Lukin, V., Vozel, B., Chehdi, K. (2015). Lossy Compression of Noisy Remote Sensing Images with Prediction of Optimal Operation Point Existence and Parameters. *SPIE Journal on Advances in Remote Sensing*, 9(1), 26. doi:10.1117/1.JRS.9.095066.

Zhai, G., Min, X. (2020). Perceptual image quality assessment: a survey. *Science China Information Sciences*, 63(11), 1–52. doi:10.1007/s11432-019-2757-1.

КЛАСИФІКАЦІЯ ЗАШУМЛЕНИХ ЗОБРАЖЕНЬ, СТИСНУТИХ З ВТРАТАМИ НА ОСНОВІ BPG

Проскура Г. А., Науменко В. В., Лукін В. В.

Кафедра інформаційно-комунікаційних технологій, Національний аерокосмічний університет, 61070 Харків, Україна

Отримані зображення дистанційного зондування можуть містити шум. Цей факт необхідно враховувати при їх стисненні з втратами та класифікації. Зокрема, при стисненні з втратами зазвичай спостерігається специфічний ефект фільтрації шуму, який може бути позитивним для класифікації. На класифікацію також може впливати методологія навчання класифікатора. У статті розглядаються особливості стиснення з втратами триканальних зображень, що спотворені шумом, за допомогою кодера покращеної портативної графіки (BPG) та їх подальша класифікація. Показано, що покращення точності класифікації даних не спостерігається, якщо стискати зображення в околі оптимальної робочої точки (OPT), а тренування класифікатора виконувати для зображень із шумом. Досліджено роботу класифікатора на основі нейронної мережі. Показано, що його навчання на стиснених даних дистанційного зондування здатне забезпечити певні переваги порівняно з навчанням на зашумлених (нестиснених) даних. У статті наведено приклади використання даних Sentinel у моделюванні.

Ключові слова: стиснення втрати зображення; оптимальна точка експлуатації; кодер BPG, класифікаційна трансформація.

Рукопис статті отримано: 09.09.2024
Надходження остаточної версії: 19.09.2024
Публікація статті: 30.09.2024